PAPER • OPEN ACCESS

Overcoming temporal dispersion for measurement of activity-related impedance changes in unmyelinated nerves

To cite this article: Ilya Tarotin *et al* 2022 *J. Neural Eng.* **19** 026054

View the article online for updates and enhancements.

Journal of Neural Engineering

PAPER

Overcoming temporal dispersion for measurement of activity-related impedance changes in unmyelinated nerves

Ilya Tarotin[1,*] , Svetlana Mastitskaya[1] , Enrico Ravagli[1] , Justin D Perkins[2], David Holder[1] and Kirill Aristovich[1]

[1] Department of Medical Physics and Biomedical Engineering, University College London, Gower Street, London WC1E 6BT, United Kingdom
[2] Clinical Science and Services, Royal Veterinary College, Hawkshead Lane, Hatfield, United Kingdom
* Author to whom any correspondence should be addressed.

E-mail: ilya.tarotin@ucl.ac.uk

Abstract

Objective. Fast neural electrical impedance tomography is an imaging technique that has been successful in visualising electrically evoked activity of myelinated fibres in peripheral nerves by measurement of the impedance changes (dZ) accompanying excitation. However, imaging of unmyelinated fibres is challenging due to temporal dispersion (TP) which occurs due to variability in conduction velocities of the fibres and leads to a decrease of the signal below the noise with distance from the stimulus. To overcome TP and allow electrical impedance tomography imaging in unmyelinated nerves, a new experimental and signal processing paradigm is required allowing dZ measurement further from the site of stimulation than compound neural activity is visible. The development of such a paradigm was the main objective of this study. *Approach.* A finite element-based statistical model of TP in porcine subdiaphragmatic nerve was developed and experimentally validated *ex-vivo*. Two paradigms for nerve stimulation and processing of the resulting data—continuous stimulation and trains of stimuli, were implemented; the optimal paradigm for recording dispersed dZ in unmyelinated nerves was determined. *Main results.* While continuous stimulation and coherent spikes averaging led to higher signal-to-noise ratios (SNRs) at close distances from the stimulus, stimulation by trains was more consistent across distances and allowed dZ measurement at up to 15 cm from the stimulus (SNR = 1.8 ± 0.8) if averaged for 30 min. *Significance.* The study develops a method that for the first time allows measurement of dZ in unmyelinated nerves in simulation and experiment, at the distances where compound action potentials are fully dispersed.

1. Introduction

Electroceuticals or bioelectronic medicines [1] are a novel emerging set of techniques aimed at treating diseases by selective stimulation of nervous tissue and neuromodulation of the internal organs innervated by it. The main nerve of interest is the vagus nerve (VNS) which is the longest autonomic nerve in the body serving as an interface between the central nervous system and major internal organs. Electrical stimulation of the VNS and neuromodulation of the internal organs or areas of the brain supplied by

it is a clinically approved technique for treatment of drug-resistant epilepsy [2, 3] and depression [4], and has a great potential for treatment of heart failure [5], rheumatoid arthritis [6] and a variety of inflammatory diseases via modulation of the cholinergic anti-inflammatory pathway [7–9]. However, despite the good clinical efficacy and great potential of VNS, it is prone to adverse effects with an incidence rate of up to 50% [10, 11] originating from non-targeted electrical stimulation of the VNS that induces modulation of all organs supplied by it leading to undesired physiological effects. To reduce side effects, selective

stimulation of the specific fascicle within the nerve leading to a particular organ in the single direction of this organ is required.

To allow selective stimulation of fascicles in the nerve, it is essential to know their precise location within this nerve. Moreover, organisation of a closed feedback loop neuromodulation of the desired organ relies on the measurement of functional activity of the fascicle supplying this organ. Both capabilities can be achieved with fast neural electrical impedance tomography (EIT), a novel method capable of imaging electrical activity in nerves in their cross-section.

1.1. Fast neural EIT

In fast neural EIT, the same as in conventional EIT, the impedance of the tissue is measured by injecting sinusoidal electric current through a pair of electrodes and recording voltages through other pairs of available electrodes [12–15]. Since the applied current amplitude is constant, the measured voltage amplitudes are directly proportional to the tissue impedance according to Ohm's law. Then, the electrode pairs are switched, and this procedure is repeated for all electrode pairs so that numerous voltage measurements with different current injections can be obtained.

EIT recordings usually contain background noise with physiological or hardware-related origin. In fast neural electrical impedance tomography, physiological noise is primarily caused by neural activity and accounts for up to 95% of total noise [16], with the remaining hardware-related noise including but not limited to thermal effects, current source noise, digitization noise and stray capacitance [17].

Using the recorded voltages, images of the internal electrical impedance of the tissue can be reconstructed by solving an inverse problem with the use of various numerical methods [12]: signal-to-noise ratio (SNR) exceeding 4 is usually required to obtain reproducible EIT images [18]. Previously, fast neural EIT was capable of reconstructing images of functional activity of the brain [13, 14] and peripheral nerves in their cross-section [12, 15, 19] with temporal and spatial resolutions of <1 ms and <200 μm respectively [12, 19]. In addition, EIT imaging in nerves was validated against micro-computed tomography and histology [19].

The physiological basis of fast neural EIT relies on a principle of activation of nerve fibres involving voltage-dependent ion channels. When a fibre depolarizes, ion channels switch to an opened state and the impedance of the tissue decreases, so that electric current which is externally applied in EIT, flows through them as the path of the least resistance. The changes usually recorded in fast neural EIT are small and equal up to 0.1%–1% of the baseline values in the brain and myelinated nerves [12, 19–21], and much smaller (<0.01%) in mammalian unmyelinated nerves [22]. This requires the noise threshold in the recordings to

be <0.01% which can theoretically be achieved using the existing EIT systems [16] if long-enough averaging of the signal is performed.

1.2. Temporal dispersion

Although fast neural EIT is reliable for imaging neural activity in the brain and peripheral nerves, imaging in autonomic nerves is more challenging for two reasons. First, autonomic nerves mainly consist of small unmyelinated C fibres [23, 24] producing lower impedance changes; second, conduction velocities (CVs) of C fibres are significantly slower and more variable [25, 26]. As a result, the amplitude of the compound action potentials (CAPs) being an aggregate sum of action potentials (APs) of individual fibres rapidly decreases along the nerve from the site of its activation. This effect is referred to as temporal dispersion (TD) [26–29] which leads to a fall of the CAP below the noise threshold beyond a few centimetres or in some cases even a few millimetres from the stimulus [22, 26, 30].

The last point is especially important for the achievement of the goals stated for bioelectronic medicines. First, mammalian, including human, VNSs are largely unmyelinated [23, 31]. Second, for selective stimulation of the specific fascicles and closed-loop neuromodulation of the internal organ which they supply, the neural activity propagating from the organ must be recorded and imaged at the cervical level. The length of the nerve from the internal organs to the neck in humans is around half a metre [32] that is significantly larger than the theoretical limit of approximately 4 cm allowed by TD in unmyelinated fibres [22]. To overcome this limitation, a method capable of measuring dZ further from the onset than allowed by TD is required.

The feasibility of this objective can partly be justified by the fact that CAPs in nerves have more pronounced phasic nature than dZs which are mainly monophasic, as was measured experimentally in crabs [33], rats [12, 19] and large animals [34] as well as confirmed in the current study (figure 6 in section 3). Therefore, the expectation is that CAPs will decrease in amplitude much faster than dZ so that dZ will be visible further from the stimulation point than CAPs are.

In addition, study [35] showed that when the stimulation paradigm had been changed from a traditional continuous nerve stimulation to application of a high-frequency series of stimuli separated by resting intervals, it was theoretically possible to record dZ at 20 cm from the stimulus with SNR of 4 if averaging for 30 min, while the traditional approach cannot be used at >5 cm [22]. However, this approach was based on a simple statistical model of an arbitrary C fibre nerve which significantly differs from real mammalian autonomic nerves. Also, the experimental parameters such as the noise, geometry of the electrodes and electrical parameters were arbitrarily

chosen based on the previously performed experiments in peripheral nerves [12].

Therefore, in order to provide accurate predictions and determine whether it was realistic to measure dZ in autonomic nerves at distances from the stimulation where CAPs were cancelled out, this approach must have been optimised. It should have accounted for realistic nerve histology and fibre composition as well as included a variety of experimental parameters utilised in impedance measurement experiments performed with mammalian nerves. Then, following the development and optimisation of the method, the predictions must have been verified experimentally.

1.3. Purpose

The main purpose of this study was to develop and optimise a method to overcome TD and allow EIT recordings of phasic activity at far distances from the onset along the nerve where compound activity is dispersed. This brings up the opportunity to image fascicles of the autonomic nerves with fast neural EIT at the distances where the CAPs fall below the noise and facilitate the development of bioelectronic medicines for selective stimulation of the VNS, neuromodulation of internal organs and treatment of associated drug-resistant disorders. Specific questions addressed in this study were as follows:

(a) What are the optimal stimulation and signal processing strategies and parameters producing the largest impedance changes at different distances (15, 20 and 50 cm) from the onset?
(b) How much averaging is required (1) to obtain a measurable signal (SNR > 1) and (2) to image neural activity with EIT (which requires SNR > 4 [18]) at 15, 20 and 50 cm from the site of stimulation?
(c) Are simulated results confirmed with the experimental data?

The first part of the study included the development of the accurate model of dispersion in the porcine subdiaphragmatic nerve (SN) which was followed by the development and optimisation of the method for overcoming dispersion and recording dZ at far distances from the stimulation site.

2. Methods

2.1. Experimental design
The study was divided into the following steps:

(a) **Development of an experimentally driven statistical model of the SN of the pig**.
The model combined (a) previously developed accurate finite element (FEM) model of a C fibre [36] and (b) statistical model for simulation of

TD of CAPs and dZs [22] in a complex nerve, consisting of a composition of unmyelinated and myelinated fibres [37]. The parameters of the model were chosen on the basis of *ex-vivo* experimental recordings (CAP and dZ) obtained using a SN of the pig subjected to repetitive continuous stimulation. As a result, the model could accurately simulate CAPs and impedance changes at ~3 cm from the stimulus and could be therefore utilized for the development and optimisation of a new method for overcoming TD and measurement dZ at further distances, where CAPs were cancelled out due to dispersion.
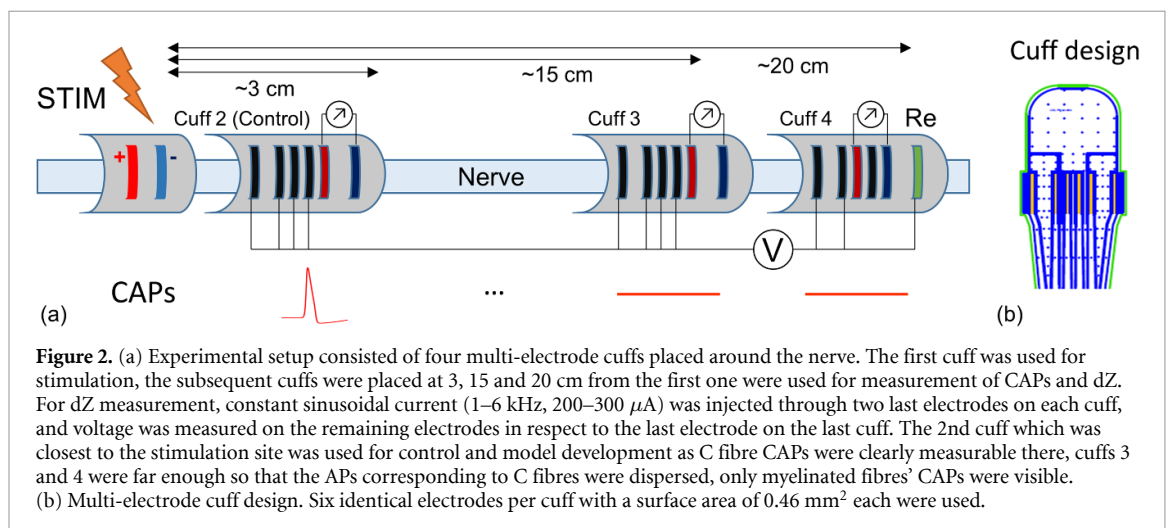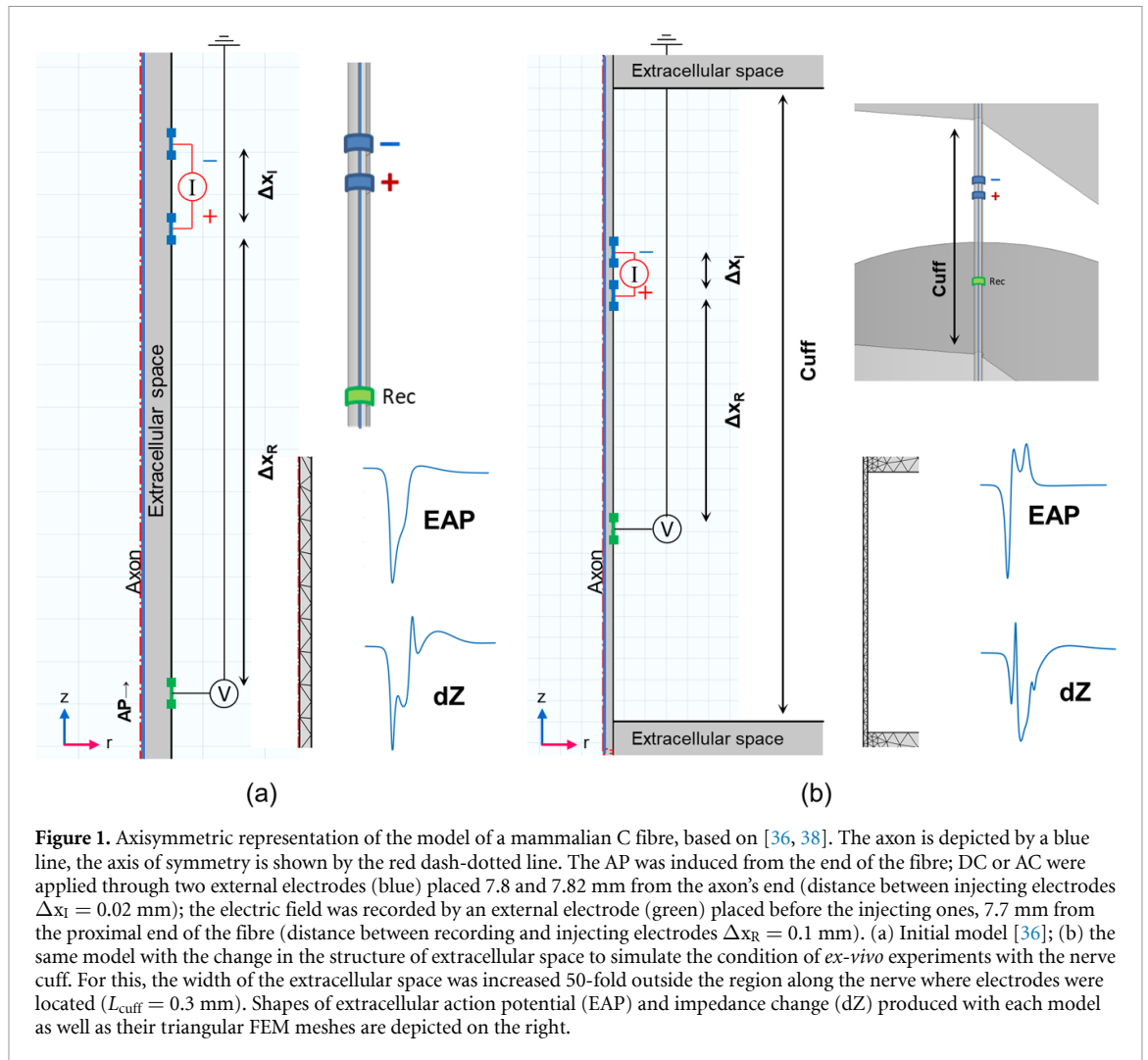
(b) **Development of a method for overcoming dispersion.**
Using the developed model, the optimal stimulation and signal processing paradigms to record impedance changes at the distances where compound APs were dispersed were obtained. For this, the modelled nerve fibre was subjected to repetitive stimuli at various frequencies. For dZ extraction, the resultant signals were processed in two ways—(1) averaging and band-pass filtering as single spikes and (2) averaging as trains of spikes allowing band-pass filtering around the whole train thus significantly reducing the bandwidth of the filter. The optimal parameters for dZ measurement at various distances from stimulation were determined, the SNR at these distances was obtained. The final predictions of the model have then been subjected to experimental verification using a preparation of the porcine SN *ex vivo* ($N = 18$).

2.2. Versatile statistical model of dispersion in nerve

2.2.1. FEM model of a single fibre
Impedance changes accompanying neural activity were obtained using the FEM models of mammalian C fibre ($d = 1 \mu$m) bi-directionally coupled with the extracellular space (figure 1) [36]. Two variants of the FEM model were designed in the study. In the first variant (figure 1(a)), the C fibre ($d = 1 \mu$m) was surrounded by a cylinder of extracellular space with the diameter equal to the one of the ring electrodes ($D = 0.01$ mm). The second variant (figure 1(b)) was designed to represent the *ex-vivo* experiments performed using multielectrode cuffs. When the silicone cuff is placed tightly around the nerve, as in the *ex-vivo* experiment performed in the current study (figure 2), there is a significantly smaller amount of saline solution inside the cuff (in the electrode-nerve interface) than along other parts of the nerve. The shape of the recorded CAP, in this case, differs from the one recorded using hook electrodes [33], where the saline solution occupies uniform volume along the nerve (as in figure 1(a)). Therefore, to simulate the activity of the C fibre in the conditions

Figure 1. Axisymmetric representation of the model of a mammalian C fibre, based on [36, 38]. The axon is depicted by a blue line, the axis of symmetry is shown by the red dash-dotted line. The AP was induced from the end of the fibre; DC or AC were applied through two external electrodes (blue) placed 7.8 and 7.82 mm from the axon's end (distance between injecting electrodes $\Delta x_I = 0.02$ mm); the electric field was recorded by an external electrode (green) placed before the injecting ones, 7.7 mm from the proximal end of the fibre (distance between recording and injecting electrodes $\Delta x_R = 0.1$ mm). (a) Initial model [36]; (b) the same model with the change in the structure of extracellular space to simulate the condition of *ex-vivo* experiments with the nerve cuff. For this, the width of the extracellular space was increased 50-fold outside the region along the nerve where electrodes were located ($L_{cuff} = 0.3$ mm). Shapes of extracellular action potential (EAP) and impedance change (dZ) produced with each model as well as their triangular FEM meshes are depicted on the right.

Figure 2. (a) Experimental setup consisted of four multi-electrode cuffs placed around the nerve. The first cuff was used for stimulation, the subsequent cuffs were placed at 3, 15 and 20 cm from the first one were used for measurement of CAPs and dZ. For dZ measurement, constant sinusoidal current (1–6 kHz, 200–300 μA) was injected through two last electrodes on each cuff, and voltage was measured on the remaining electrodes in respect to the last electrode on the last cuff. The 2nd cuff which was closest to the stimulation site was used for control and model development as C fibre CAPs were clearly measurable there, cuffs 3 and 4 were far enough so that the APs corresponding to C fibres were dispersed, only myelinated fibres' CAPs were visible. (b) Multi-electrode cuff design. Six identical electrodes per cuff with a surface area of 0.46 mm² each were used.

similar to those when the cuff is present, the width of the extracellular space cylinder was increased 50-fold outside the 0.3 mm region along the nerve where electrodes were located (figure 1(b)).

The electric field in the extracellular space was simulated using volume conduction Poisson's

equation, and the fibre was modelled using the conductance-based Hodgkin–Huxley type Tigerholm model of a mammalian C nociceptor [38]. The Tigerholm model was chosen as it could accurately represent the active behaviour of mammalian C fibre (porcine SNs mainly consist of C fibres [31]) and was

validated experimentally [38]. In addition, the model has previously shown itself capable of optimising experimental parameters for obtaining the largest impedance changes in unmyelinated nerves as well as explaining the biophysical origin of experimental recordings [36].

The Tigerholm model contained ten ion channels and variable concentrations inside and outside of the fibre; these concentrations, together with other parameters, affected the membrane conductance which, in turn, led to changes in electric potentials inside and outside the membrane (equations (27) and (28) in the supplementary material of [36]). The impedance change (dZ) signal measured in the model is related to a change in the membrane conductance which is, among other parameters, influenced by variable extra- and intracellular ionic concentrations.

For measurement of impedance change, constant direct current of small amplitude (1.25 μA, or 4 mA cm^{-2}) was continuously applied to the fibre during stimulation through two external ring electrodes. The reason was that using DC was less computationally intensive than AC, especially at high frequencies, and it was previously shown that dZ obtained with small amplitude DC and AC had the same biophysical origin [36].

Voltage was measured simultaneously using the recording electrode placed before the injecting ones with respect to ground (figure 1), the same as in [36]. Since the constant current was applied, and because the phase shift $\Delta\varphi$ between the injected current and measured voltage is close to zero [34, 39], the measured impedance change dZ may be expressed as follows:

$$dZ = \frac{Z(t) - Z(t_{AP})}{Z(t)} = \frac{|V(t)|e^{j\Delta\varphi} - |V(t_{AP})|e^{j\Delta\varphi_{AP}}}{|V(t)|e^{j\Delta\varphi}}$$

$$\approx \frac{|V(t)| - |V(t_{AP})|}{|V(t)|} = |dZ|. \tag{1}$$

In the equation, impedance change dZ is equal to the relative change of the impedance $Z(t_{AP})$ when AP passes under the electrodes with respect to the baseline impedance of the system $Z = Z(t)$. Using (1), the complex dZ and absolute |dZ| can be expressed in terms of the measured voltages $V = V(t)$ and $V(t_{AP})$.

To extract dZ, DC was applied twice in different polarities with positive and negative electrodes switched [36]. These voltage signals were subtracted from each other so that the identical APs were cancelled out, while the dZ which modulates the recorded voltage, doubled, and could be easily extracted. In the experiments performed in the study, this subtraction step was not required as high AC frequencies ($\geqslant$2 kHz) were used and CAPs were removed by bandpass filtering around the carrier frequency (as the characteristic frequency of the CAP is <1 kHz [40]) (figure 4).

The parameters and geometrical design of the model as well as all the equations describing it can be found in [36].

2.2.2. Statistical model of a complex nerve
The APs and impedance changes (dZs) obtained with the FEM model were incorporated into the statistical model for simulation of the dispersed compound signals of a multi-fibre porcine SN. The modelled nerve included 40 000 unmyelinated C fibres and 4000 fast myelinated fibres [37] fibres uniformly distributed in the cross-section of the nerve, with normally distributed CVs (table 2). Normal distribution of the CV was considered based on the histological studies in various nerves [23, 41, 42] where the distributions of fibres' diameters (which are directly proportional to CVs [22]) close to normal were obtained; the same assumption was also made in the recent modelling study [22].

The compound dZ was obtained as the sum of single impedance changes of each fibre at the required distance from the site of stimulation:

$$CAP(x,t) = \sum_{i=1}^{N_C = 40\,000} EAP_i^C(x,t) + \sum_{i=1}^{N_M = 4000} EAP_i^M(x,t)$$

$$dZ(x,t) = \sum_{i=1}^{N_C = 40\,000} dZ_i^C(x,t) + \sum_{i=1}^{N_M = 4000} dZ_i^M(x,t) \tag{2}$$

where CAP and dZ are APs and impedance changes of the compound nerve, EAP_i^C, EAP_i^M, dZ_i^C and dZ_i^M represent single extracellular AP and dZ corresponding to C fibres and myelinated fibres respectively (figure 1).

Due to the difference in geometric and electrical parameters utilised in the single-fibre FEM and the experimentally-based statistical multiple-fibre model, the single APs and dZs simulated with the FEM model (subsection A) were scaled in amplitude before summation, as in [22]. However, compared to [22] where electrode diameter and connective tissue resistivity were only considered, multiple parameters differing between the FEM and statistical models were introduced, so that the predictions of the final model closely agree with experimental data.

For scaling, the obtained extracellular AP and dZ were multiplied by the coefficients $k_{AP} = \prod_i k_{APi}$ and $k_{dZ} = \prod_i k_{dZi}$, where k_{APi} and k_{dZi} accounted for various parameters that differed in the FEM and statistical models and affected AP and dZ respectively:

$$EAP_{stat} = k_{AP} \cdot EAP_{FEM}$$

$$dZ_{stat} = k_{dZ} \cdot dZ_{FEM}. \tag{3}$$

The considered parameters affecting the dZ were [36]: the electrodes' diameter (d), extracellular resistivity

(ρ), the current density of the applied dZ measuring current (J), the distance between recording and injecting electrodes (Δx_R, figure 1), the distance between injecting electrodes (Δx_I, figure 1). The latter three parameters were found to strongly influence the dZ measurements in the previously performed study [36]. For scaling APs, the electrodes' diameter (distance between the electrode and the fibre) and conductivity of the extracellular space were considered, as other parameters did not have any effect on its value. The final equations for scaling APs and dZs are presented below:

$$k_{AP} = \left(\frac{d_{FEM}}{(1 - 1/\sqrt{2}) \cdot d_{stat}} \right)^3 \cdot \frac{\rho_{stat}}{\rho_{FEM}} \quad (4)$$

$$k_{dZ} = \left(\frac{d_{FEM}}{(1 - 1/\sqrt{2}) \cdot d_{stat}} \right)^4 \cdot \left(\frac{\rho_{stat}}{\rho_{FEM}} \right)^2 \cdot \frac{J_{stat}}{J_{FEM}}$$

$$\cdot \frac{dZ_{\Delta x_{R_{stat}}}}{dZ_{\Delta x_{R_{FEM}}}} \cdot \frac{dZ_{\Delta x_{I_{stat}}}}{dZ_{\Delta x_{I_{FEM}}}}. \quad (5)$$

In the equations, index *stat* corresponds to the value used in the experiments and in the statistical model, and *FEM*—in the FEM model. The detailed strategy for evaluation of the scaling coefficients as well as their values are presented in supplementary material (available online at stacks.iop.org/JNE/19/026054/mmedia) and in table 1(A).

In addition to the introduced scaling coefficients, CVs of the fibres in the model were chosen so that simulated CAP and dZ closely match the experimental ones recorded using the *ex vivo* preparation of the porcine SN. The porcine SN mainly consists of unmyelinated C fibres and is a good representation of the subdiaphragmatic branches of human VNSs [31].

For the preparation, nerves of 20–25 cm length were sourced from the terminally anaesthetized pigs used in other experimental studies. The nerves were held in an organ bath perfusion chamber filled with oxygenated Krebs-Ringer solution kept at ∼30 °C. Three silicone rubber cuffs with six radially arranged electrodes each were placed around the nerve 3, 15 & 20 cm from a cuff for electrical stimulation so that the TD of CAPs can be observed (figures 2(a) and (b)). The stainless-steel electrodes (0.2 × 2.3 mm², figure 2(b)) embedded into a medical-grade silicone rubber base were fabricated using a laser cutter and coated with PEDOT:pTS providing the lowest contact impedance and phase shift (∼300 Ω and 1.5° at 1 kHz) among the popular coating electrode materials [34].

The choice of six-electrode design was done (1) for verification purposes—dZ must be equal on electrodes 1–4 if the measuring current is applied through electrodes 5 and 6, and (2) to account for possible failures of one or more electrodes on the cuff. These may have happened due to multiple reasons including un-soldered connection, broken wire, increased contact impedance due to initially low-quality or detached PEDOT:pTS coating as well as bad contact of the particular electrode and the nerve.

With the designed setup, dZ and CAPs were recorded using the 2nd cuff placed at approximately 3 cm from the site of the onset with respect to the electrode on the last cuff using continuous stimulation with frequency $f_{stim} = 2$ Hz, current $I_{stim} = 20$–40 mA depending on the thickness of the nerve, pulse width PW = 50 μs, frequency and amplitude of the applied impedance measuring current $f_{AC} = 1$–6 kHz, $I_{AC} = 200$–300 μA (28 nerves in total).

To obtain satisfactory SNR, averaging was required; for this purpose, CAPs were recorded for 20 s, and the dZ—for 10 min. Based on the recorded CAP and dZ, the CV (mean and S.D.) of the fibres constituting the statistical model were determined. This was done using times of the negative peaks of the CAPs related to fast (Ab) and slow (C) fibres as well as their widths. Knowing the distances of the recording cuff from the stimulation, the CV could be calculated.

The average level of the Gaussian noise present in the *ex-vivo* experiments (3.5 μV RMS before averaging) was added to the resultant modelled signals as the last step. Addition of noise allowed to determine the optimal parameters for maximisation of the SNR, defined as the amplitude of the signal divided by the standard deviation of the noise. The optimal parameters to be determined include, among others, the bandwidth of filtering which will be influenced by type and levels of noise present in the recordings.

The resulting finalised model could utilise EAP and dZ produced with the FEM model (figure 1(b)) subjected to an arbitrary stimulation paradigm and, on this basis, it could accurately predict values of CAP and dZ produced by the porcine SN at any distance from the onset of the stimulus. Therefore, the model is versatile and could be used to determine the optimal stimulation paradigm for overcoming dispersion and recording dZ further than CAPs are visible.

The COMSOL and MATLAB model files used for FEM and statistical modelling are provided online in the EIT-lab GitHub repository.

2.3. A method for overcoming TD in autonomic nerves

2.3.1. Model setup

The developed model was utilised to determine the optimal paradigm for dZ measurement at various distances from the stimulation site where CAPs are

Table 1. Initial stimulation and processing parameters used in the model.

Parameter	Value					
Stimulation (train) frequency	1 Hz	2 Hz	5 Hz	10 Hz	20 Hz	50 Hz
$N_{spikes/train}$	10	20	40	24	14	10
Duration of the train	10 s	10 s	8 s	2.5 s	0.75 s	0.25 s
Time between trains	0 s (continuous)			3 s		
Duration of the simulation			30 min			
$N_{trains/30\,min}$	180	180	163	327	480	553
Filtering bandwidth (single pulses)			200 Hz			
Theoretical bandwidth (trains)	0.2 Hz	0.2 Hz	0.25 Hz	0.8 Hz	2.7 Hz	8 Hz
Distances of measurement			3, 15, 20, 50 cm			

dispersed (>5 cm from the stimulus in mammalian unmyelinated nerves [22]).

For this, the FEM model of a C fibre (figure 1(b)) was subjected to series of repetitive bipolar monophasic stimuli (50 μs pulse width, 5 nA) which were applied intracellularly across 0.1 mm at the end of the fibre. Two stimulation paradigms were used (figure 3(a)): (1) continuous stimulation with the frequency of 1 and 2 Hz (at these frequencies, the fibre never loses the ability to excitation); (2) stimulation with trains of stimuli of 5, 10, 20 and 50 Hz separated by resting intervals to allow the nerve recovery between the consecutive trains (table 1).

During repetitive stimulation at 5–50 Hz, the amplitudes of the consecutive APs were decreasing until the fibre lost the ability to excitation (figure 3(b)) that also happens experimentally due to the accumulation of potassium ions in the periaxonal space adjacent to the membrane [44, 45]. Therefore, in case stimulating trains would last longer than the nerve is capable to be activated, the ratio of nerve firing time to the duration of the stimulation (duty cycle) would be reduced.

Thus, durations of the trains were chosen so that (1) the time when the nerve is in the active state (and hence the dZ) is maximised, that includes maximisation of the number of APs per train and the duty cycle, and (2) the nerve survives for the long term (>∼3 h in the saline bath) in the *ex-vivo* experiment (figure 2(a)), as increasing SNR to satisfying values may require prolonged averaging. The maximal durations allowing reaching the highest duty cycle were 8, 2.5, 0.75 and 0.25 s at 5, 10, 20 and 50 Hz respectively that was equal to 40, 24, 14 and 10 spikes per train at these frequencies (table 1). The resting time T_{rest} between the 5–50 Hz trains was chosen to be 3 s (figure 3(a) and table 1).

In order to achieve long-term survival of the stimulated nerves so that they are stable during the experimental day period (CAPs are not changing for >6 h), these parameters were adjusted following testing performed in three nerves (table 3 in section 3). For this, CAP amplitudes in the nerves were extracted following their initial stimulation with the maximal train durations provided above and in table 1. Then, if the CAPs' amplitudes did not sustain for the duration of

the experiment, the number of pulses and associated train durations were halved—this was repeated up to two times until the CAPs stable over several hours were achieved. To further improve stability, the resting time was also iteratively increased and its effect on the CAPs were observed.

In contrast to the APs, the amplitudes of the single-fibre impedance changes were increasing during stimulation (figure 3(c)). The reasons for this behaviour are supposedly similar to the ones for the APs (figure 3(b)): accumulation of potassium ions in the periaxonal space and sodium ions inside the fibre modifies reversal potentials of these ions and sensitises the associated ion channels thus leading to increased total conductance of the fibre during excitation. This effect is expected to improve the experimental dZ response during repetitive stimulation. However, it is hard to evaluate it experimentally since at least 1200 averages are required to reliably detect single spike dZ (10 min averaging at 2 Hz stimulation, section 2.2.2), and this would average out the progressively increasing dZ amplitudes. In addition, the number of spikes in the train and the resting time between trains was found to significantly affect nerve survival (6 pulses/train, 5 s between trains, table 3 in section 3)—it was vital for the purposes of the study, and the gradually increasing behaviour of dZ had therefore not been investigated further.

The obtained dZ trains (figure 3(c)) were incorporated into the statistical model for simulation of the dispersed compound dZ of a multi-fibre nerve described in the previous subsection. The SNR (ratio of mean signal to S.D. of the noise) at 3, 15, 20 and 50 cm from the onset of the stimulus was determined using two signal processing paradigms described in the next subsection. For averaging and noise reduction, the total duration of each simulation was chosen to be 30 min (table 1). 50 models were simulated in total to obtain statistics.

2.3.2. Signal processing
To extract compound impedance changes from the dispersed signals obtained in the statistical model, the following signal processing paradigms were performed; SNRs using these paradigms were obtained.
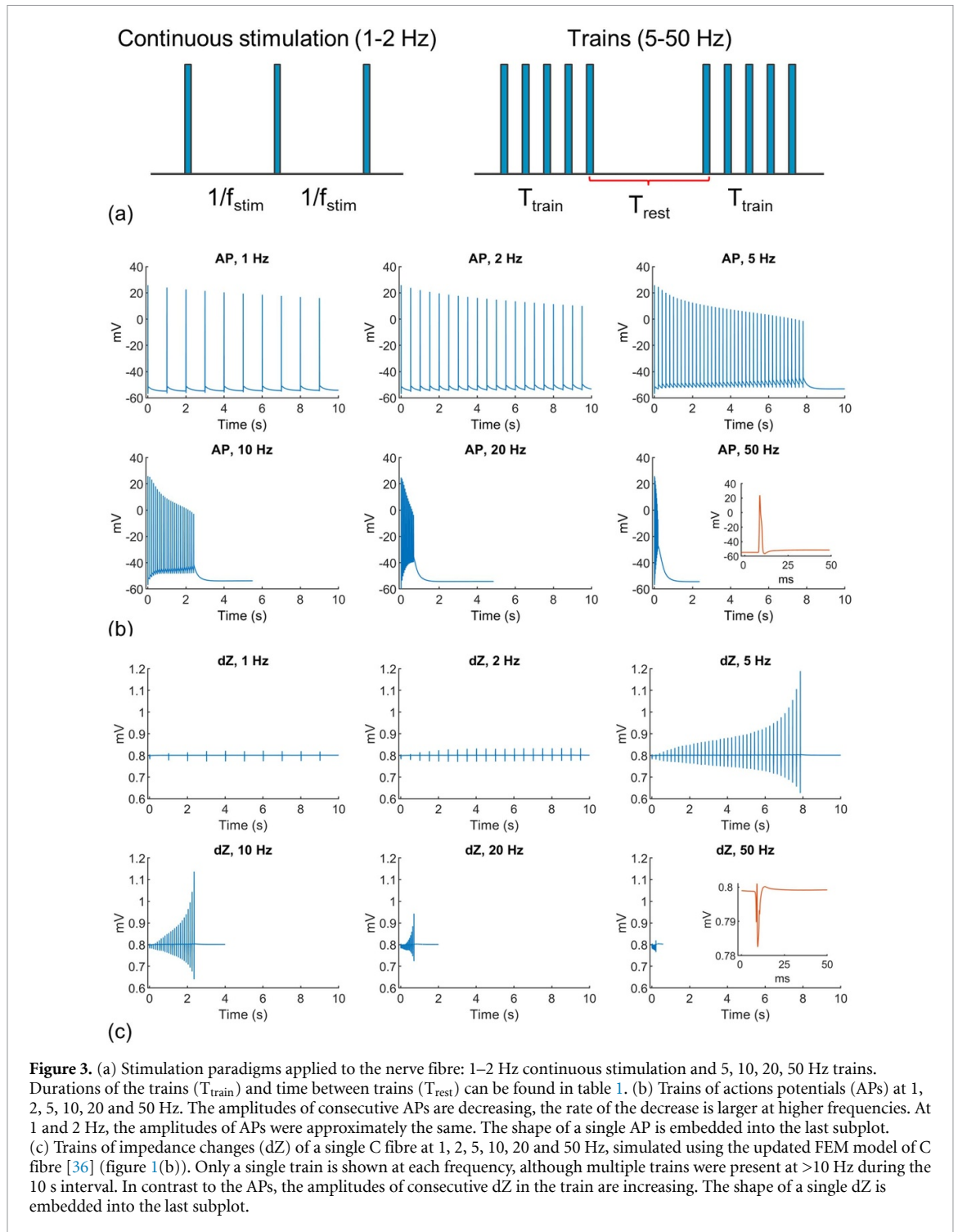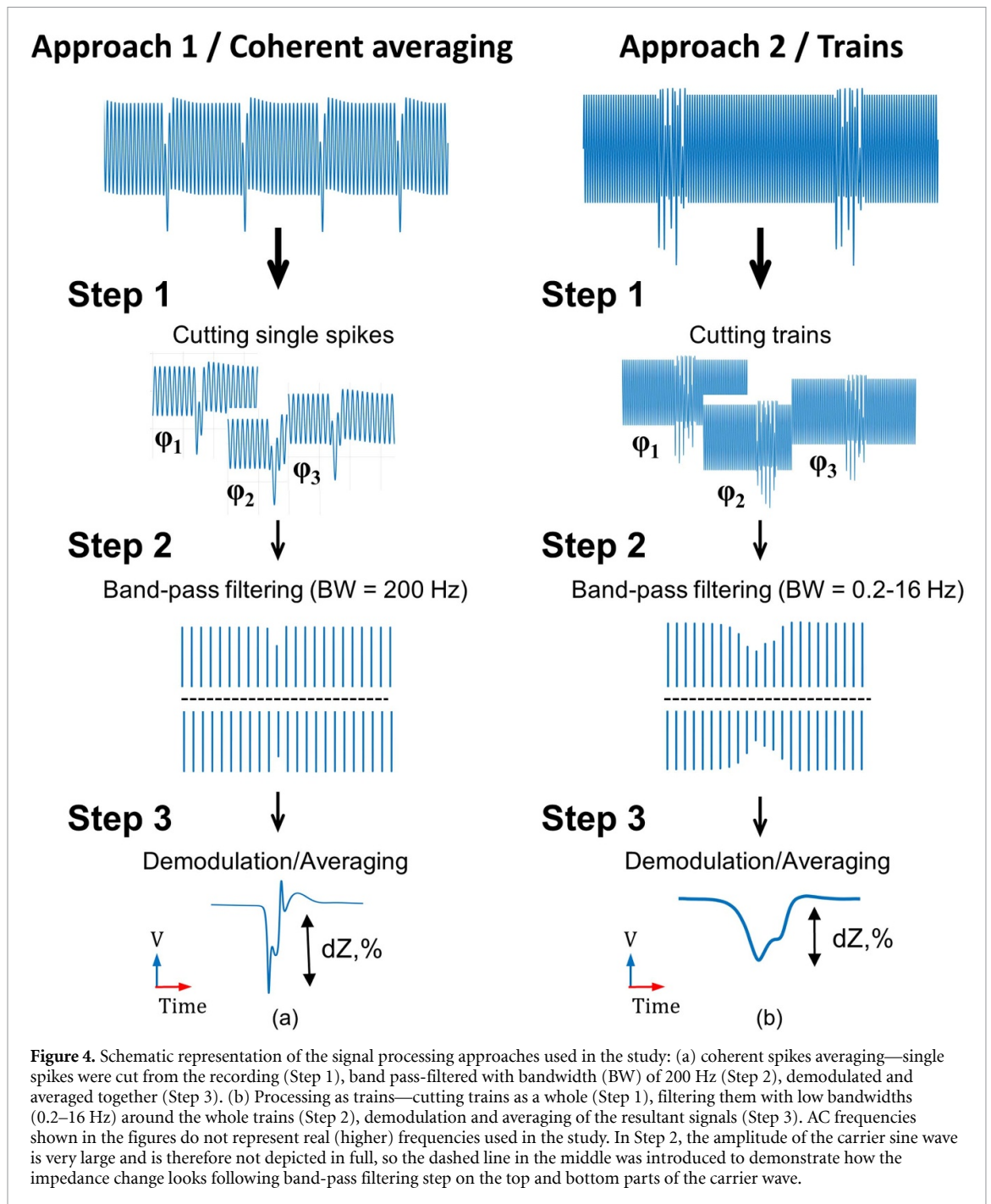
Figure 3. (a) Stimulation paradigms applied to the nerve fibre: 1–2 Hz continuous stimulation and 5, 10, 20, 50 Hz trains. Durations of the trains (T_{train}) and time between trains (T_{rest}) can be found in table 1. (b) Trains of actions potentials (APs) at 1, 2, 5, 10, 20 and 50 Hz. The amplitudes of consecutive APs are decreasing, the rate of the decrease is larger at higher frequencies. At 1 and 2 Hz, the amplitudes of APs were approximately the same. The shape of a single AP is embedded into the last subplot. (c) Trains of impedance changes (dZ) of a single C fibre at 1, 2, 5, 10, 20 and 50 Hz, simulated using the updated FEM model of C fibre [36] (figure 1(b)). Only a single train is shown at each frequency, although multiple trains were present at >10 Hz during the 10 s interval. In contrast to the APs, the amplitudes of consecutive dZ in the train are increasing. The shape of a single dZ is embedded into the last subplot.

(i) *Averaging of single spikes (coherent spikes averaging).* This approach has traditionally been used in previous studies involving dZ measurement [12, 15, 19, 33]. In those studies, the recordings were cut into single spikes segments with the time window corresponding to the stimulation frequency around each spike (figure 4(a)). Those segments were then (1) band-pass filtered using the bandwidths of 100–3000 Hz depending on the characteristic frequency of these signals (characteristic frequency of A fibres ≫ C

fibres), (2) demodulated using the absolute of Hilbert transform (since the phase shift induced by the membrane is insignificant [34, 36], and the dZ is approximately equal to |dZ|, equation (1) and (3) averaged together. In the current study, BW was chosen to be 200 Hz to account for the characteristic frequency of the simulated non-dispersed dZ (figure 1). The resulting signals were averaged across all 50 computed models. SNR was calculated using the formula:

Figure 4. Schematic representation of the signal processing approaches used in the study: (a) coherent spikes averaging—single spikes were cut from the recording (Step 1), band pass-filtered with bandwidth (BW) of 200 Hz (Step 2), demodulated and averaged together (Step 3). (b) Processing as trains—cutting trains as a whole (Step 1), filtering them with low bandwidths (0.2–16 Hz) around the whole trains (Step 2), demodulation and averaging of the resultant signals (Step 3). AC frequencies shown in the figures do not represent real (higher) frequencies used in the study. In Step 2, the amplitude of the carrier sine wave is very large and is therefore not depicted in full, so the dashed line in the middle was introduced to demonstrate how the impedance change looks following band-pass filtering step on the top and bottom parts of the carrier wave.

$$SNR_{single} = A_{signal}/\sigma_{Noise} \qquad (6)$$

where A_{signal} is the maximal amplitude of the measured signal, σ_{noise} is the standard deviation of the noise after filtering.

(ii) *Processing trains of spikes as a whole.* Instead of cutting the recordings into single spikes, processing was conducted on the entire trains of spikes (figure 4(b)). This allowed band-pass filtering with bandwidths around whole trains lasting up to a few seconds. As a result, the theoretical bandwidths for band-pass filtering could be significantly lower at 0.2–8 Hz, determined as $BW_2 = 2/T_{train}$ where T_{train} is the duration of the specific train (table 1). This could allow a significant reduction of the noise without long-continued averaging. However, to differentiate the dZ signal of the C fibres from the signal of myelinated fibres, stimulation artefacts and low-frequency noise present in the recordings, these theoretical filtering bandwidths had to be increased (table 3 in section 3).

SNR at 3, 15, 20 and 50 cm from the onset of the stimulus was computed according to (6), where A_{signal} and σ_{noise} corresponded to a new approach for signal processing. Due to the presence of stimulation artefacts (see the detailed description below) as well as fast myelinated

fibres in the experimental recordings (figures 7 and 9), only the ending portions of the dispersed dZ corresponding to the slow C fibres could be recovered. Therefore, the last 100–500 ms in the processed dispersed dZ trains were considered for dZ and SNR calculation (figure 8 in the section 3). Although only the ending portions of the signals were used to measure dZ, the entire spike train signals were filtered: leaving the dZ in the central part of the signal allowed avoiding the filtering edge artefacts. Another artefact appearing due to presence of spikes at the end of the train when filtering the whole signal was of much shorter duration (in the order of tens of milliseconds) than the expected and observed dispersed dZ signal lasting up to 500 ms (figure 8), so they could be easily differentiated. Based on the obtained results, the optimal stimulation paradigm for recording dZ at far distances from the stimulus was determined.

Stimulation artefacts are inevitable when neural activity is evoked and recorded with the use of external electrodes [12, 19, 33]. Since the membrane of nerve fibres is more resistive than the surrounding connective tissue and physiological solution interface, part of the current applied during stimulation will flow through the conductive pathways along the nerve and an increase in the potential will be therefore measured by the recording electrodes (figure 5). In addition, the voltage generated by the stimulation current is usually orders of magnitude higher than the recorded physiological voltages, so, the insufficient input range of the amplifier or small charge imbalance between stimulation electrodes may lead to saturation of the recording circuits which can last significantly longer than stimulation pulse itself [46, 47]. To avoid saturation in the current study, charge-balanced biphasic stimulation was used together with an actiCHamp amplifier (Brainproducts GmbH, Gilching, Germany) having a wide input range of ±400 mV [16].

The influence of stimulation artefact can generally be minimised by placing the recording electrodes as far from the stimulating ones as possible. This is challenging in *ex vivo* conditions: surgically, it was not possible to extract intact undamaged SNs longer than ~20 cm from the anesthetised pig in the current study. However, *in vivo* approach is much more promising as stimulation and recording can be done in different parts of the VNS (cervical and subdiaphragmatic); this is an essential part of the future work (see Discussion).

Stimulation artefacts obtained in the current study were nonsaturating [46] so that they could be minimised, and genuine CAP and dZ signals could be extracted through filtering. However, these artefacts could not be completely eliminated that severely affected signal processing in the case when the nerve was stimulated by trains of spikes (figure 4(b)): only ending parts of the dispersed dZ signals had to be studied and the SNR could have therefore been reduced (see sections 3 and 4).

2.3.3. Experimental evaluation of the method using porcine SN ex vivo

All experimental procedures complied with regulations in the UK Animal (Scientific Procedures) Act, 1986 and were reviewed and approved by the Animal Welfare and Ethical Review Board. For experimental evaluation of the developed method, an *ex-vivo* setup with the SNs of the pig was used. In addition to porcine SNs being similar in fibre composition to the subdiaphragmatic branches of the VNSs in humans [31], they are very endurant—the stability of porcine SNs allowed to frequently manipulate them in the saline bath and conduct experiments lasting for more than 8 h, in accordance with survival times of other mammalian nerves [48, 49]. This is a significant advantage over other unmyelinated nerves commonly used in *ex-vivo* setting such as a walking leg nerve of the crab [33, 50] (figure A2 in supplementary material).

The experimental design was the same as in section 2, (b) describing the experimental adjustment of the model. Shortly, porcine SN were held in an organ bath perfusion chamber filled with continuously oxygenated saline solution. Three silicone rubber cuffs each having six radially arranged electrodes made from stainless steel and coated with PEDOT:pTS were placed around the nerve 3, 15 & 20 cm from the same cuff used for electrical stimulation (f_{stim} = 2 Hz, I_{stim} = 20–40 mA, PW = 50 μs, figure 2(a)). Impedance changes were measured by sequential application of the sinusoidal current through two last electrodes on each cuff, and the voltage was recorded on the remaining electrodes on the same cuff in respect to the last electrode on the last cuff (figure 2(a)). Then, dZ was obtained by demodulation of the recorded voltage using the absolute of the Hilbert transform (1). Parameters of the applied sinusoidal current were: f_{AC} = 1–6 kHz, I_{AC} = 200–300 μA.

The optimal stimulation paradigm for recording dispersed dZ determined with the model was applied to $N = 28$ nerves to sequentially record dZ using cuffs 3 and 4 at 15 and 20 cm from the onset, where CAPs were dispersed and not measurable (figure 2(a)). SNRs at these distances were obtained; implications for imaging unmyelinated nerves with fast neural EIT were investigated.

Statistical significance of the recorded dZ was verified using a two-sample t-test algorithm by comparison of the measurement amplitude straight after the stimulation artefacts (600–1000 ms, figure 8) with the dZ at all other points following this period (1000–3000 ms).
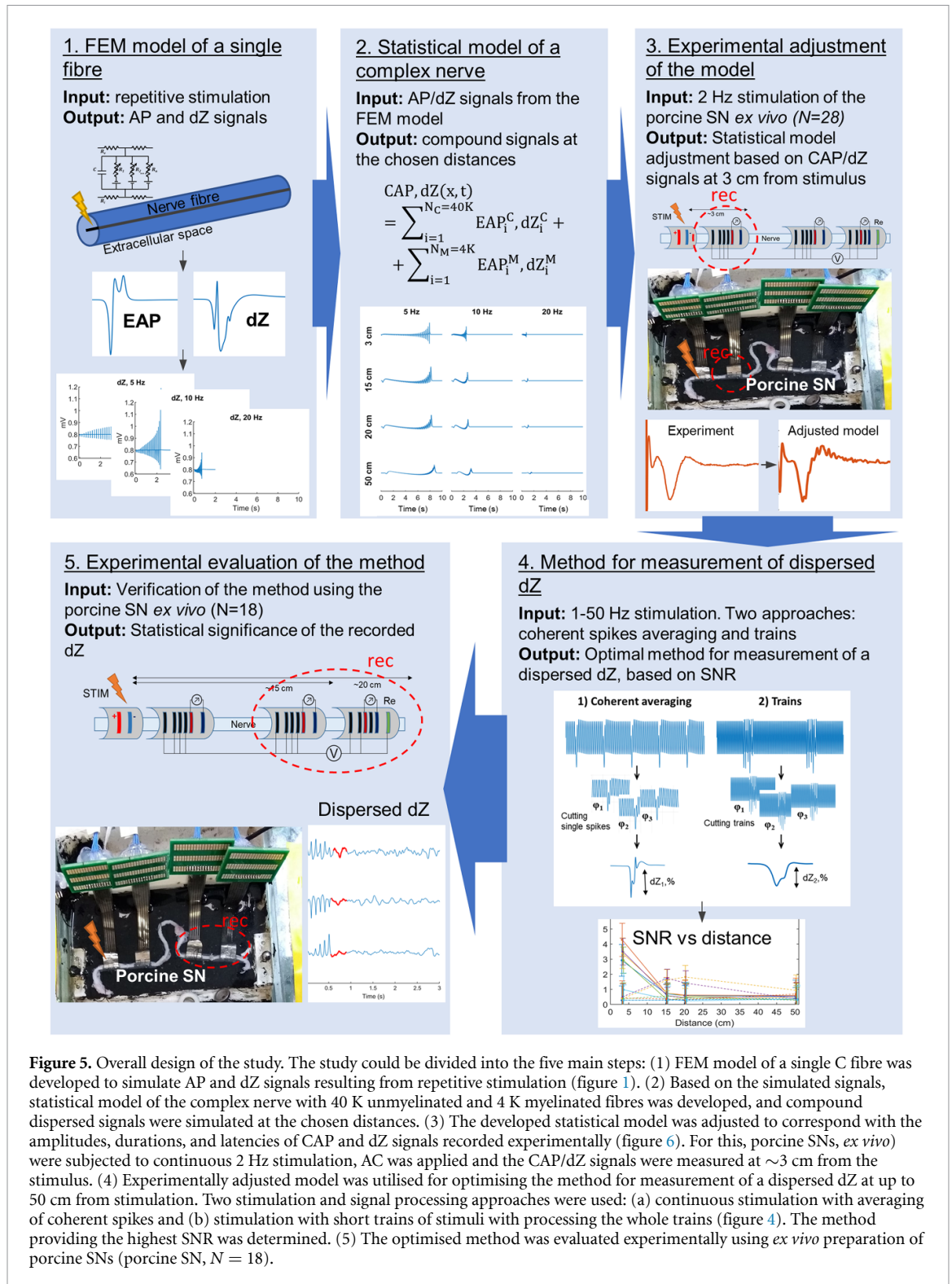
Figure 5. Overall design of the study. The study could be divided into the five main steps: (1) FEM model of a single C fibre was developed to simulate AP and dZ signals resulting from repetitive stimulation (figure 1). (2) Based on the simulated signals, statistical model of the complex nerve with 40 K unmyelinated and 4 K myelinated fibres was developed, and compound dispersed signals were simulated at the chosen distances. (3) The developed statistical model was adjusted to correspond with the amplitudes, durations, and latencies of CAP and dZ signals recorded experimentally (figure 6). For this, porcine SNs, *ex vivo*) were subjected to continuous 2 Hz stimulation, AC was applied and the CAP/dZ signals were measured at ∼3 cm from the stimulus. (4) Experimentally adjusted model was utilised for optimising the method for measurement of a dispersed dZ at up to 50 cm from stimulation. Two stimulation and signal processing approaches were used: (a) continuous stimulation with averaging of coherent spikes and (b) stimulation with short trains of stimuli with processing the whole trains (figure 4). The method providing the highest SNR was determined. (5) The optimised method was evaluated experimentally using *ex vivo* preparation of porcine SNs (porcine SN, $N = 18$).

The overall design of the study, including the workflow from development of the models to experimental verification, is presented in figure 5.

The MATLAB code written for data processing is provided in the EIT-lab GitHub repository; all the recorded unprocessed data will be available online in the SPARC portal (https://sparc.science/) after approval.

3. Results

3.1. Experimental adjustment of the statistical model of the porcine SN

Initial recordings of CAPs and impedance changes at 3 cm from the stimulation site (cuff 2, $N = 28$ nerves, figure 2(a)) allowed adjusting the statistical model to correspond to experimental data (figure 6 and table 2).

Table 2. Main parameters of the statistical models.

Parameter	Modified statistical model
C fibres number	40 000
C fibres CV	0.8 ± 0.3 m s^{-1}
Myelinated fibres number	4000
Myelinated fibres CV	8 ± 3 m s^{-1}
Noise, RMS before averaging	$3.5\ \mu$V

The CAPs recorded at cuff 2 were equal to $34 \pm 17\ \mu$V for myelinated fibres and $69 \pm 44\ \mu$V for unmyelinated fibres (mean $\pm$ s.d., figure 6(a)). The peak of myelinated fibres CAP was observed on average at 5 ms from the stimulus, peak of C fibres CAP—at 30 ms from the stimulus that allowed to determine their CVs: $v_{fast} = 8 \pm 3$ m s^{-1}, $v_C = 0.8 \pm 0.3$ m s^{-1} (mean $\pm$ s.d., table 2). The amplitude of the CAP of fast myelinated fibres was lower in the experiment than in the model because part of it was covered by stimulation artefact thus decreasing its amplitude (figure 6(a)). The dZ were equal to $(1.42 \pm 1.11) \times 10^{-4}$% ($0.16 \pm 0.19\ \mu$V) and $(6.96 \pm 4.61) \times 10^{-4}$% ($0.74 \pm 0.58\ \mu$V) in fast myelinated fibres and unmyelinated C fibres respectively.

3.2. Optimisation and experimental evaluation of the method for measurement of the dispersed dZ

3.2.1. Method development and optimisation
Using the designed statistical model of dispersion in the porcine SN, the method for recording dZ further from the site of the onset than CAPs are measurable was developed and optimised.

Images of the dispersed dZ with and without fast myelinated fibres (the real porcine SN case and artificial unmyelinated case) show that the C fibre activity is more dispersed and constitute a low-frequency component in the resultant signal, while myelinated fibres correspond to a high-frequency component (figure 7, blue and red lines). Therefore, to measure dZ of the C fibres in the mixed porcine SN nerve, the ending parts of the signals were considered.

By stimulation of three nerves with trains of pulses of 5, 10, 20 and 50 Hz with 3 s intervals between trains, and following the approach described in section 2.3.1, it was found that to achieve long-term (>6 h) survival of the nerves, the number of pulses in each train must not exceed six and the interval between trains must be increased to 5 s, independent of the applied train frequency. The model was modified accordingly (table 3).

The developed model has shown that the SNR obtained using the coherent spike averaging approach for signal processing (table 1 and figure 4(a)) were larger at short distances from the onset while falling exponentially at longer distances (solid lines in

figure 8 and table 4). The second approach involving processing of whole trains (table 1 and figure 4(b)) led to smaller SNR at 3 cm from the stimulus, but increased to >1 at 15 and 20 cm from the site of the stimulus after 30 min of averaging (figure 8 and table 4).

Therefore, the optimal parameters for measurement of dZ at far distances from the site stimulation predicted with the model were: stimulation with 5 or 10 Hz trains, six pulses per train, 5 s interval between trains (table 4). Filtering bandwidth was increased to 10 Hz to differentiate the dZ signal of the C fibres from the signal corresponding to myelinated fibres, stimulation artefacts and low-frequency noise present in the recordings (figures 7 and 9).

Even with the optimal parameters, averaging for 30 min only produces SNR marginally higher than the limit of detectability at 15 and 20 cm from the stimulus (1.8 ± 0.8 at 10 Hz, 15 cm, table 4). Therefore, to measure dZ at longer distances as well as to obtain an SNR of 4 which is minimally required for reproducible imaging of fast impedance changes with EIT [18], longer averaging will be required (see Discussion for details).

3.2.2. Experimental evaluation of the developed approach
The optimal stimulation and signal processing paradigm for recording dispersed dZ in unmyelinated fibres determined in the modelling study (10 Hz trains, 6 pulses/train, 5 s interval between trains, filtering bandwidth 10 Hz) were applied to 28 porcine SNs *ex-vivo*, out of which $N = 18$ recordings had a satisfactory level of noise smaller than $4\ \mu$V RMS before averaging, in agreement with the developed modified model.

For each nerve, the dZ measurement was sequentially performed using cuff 3 and cuff 4, located at 15 and 20 cm from the site of stimulation respectively (figure 2). Due to the presence of fast myelinated fibres and stimulation artefacts in the recordings (figures 7 and 9), measurements were done at the ending stages of the dispersed dZ, from 0.6 to 1.1 s and from 0.65 to 1.15 s for the used 10 Hz trains at cuff 3 and cuff 4 respectively (figure 7(b)).

The resulting dZ were equal to $(1.11 \pm 1.03) \times 10^{-4}$% ($0.11 \pm 0.10\ \mu$V) at 15 cm (cuff 3, figure 2(a)), and $(1.17 \pm 1.21) \times 10^{-4}$% ($0.12 \pm 0.10\ \mu$V) at 20 cm (cuff 4, figure 2(a)) from the site of stimulation. The SNR at 15 cm after 30 min of averaging was 1.8 ± 0.7, decreasing to 1.7 ± 0.6 at 20 cm that is in agreement with the predictions of the developed model (figure 8(b) and table 4). The mean absolute value of the determined dZ across all nerves was found to be significantly larger than the mean at every other point in the recording ($P < 0.01$, $N = 18$).
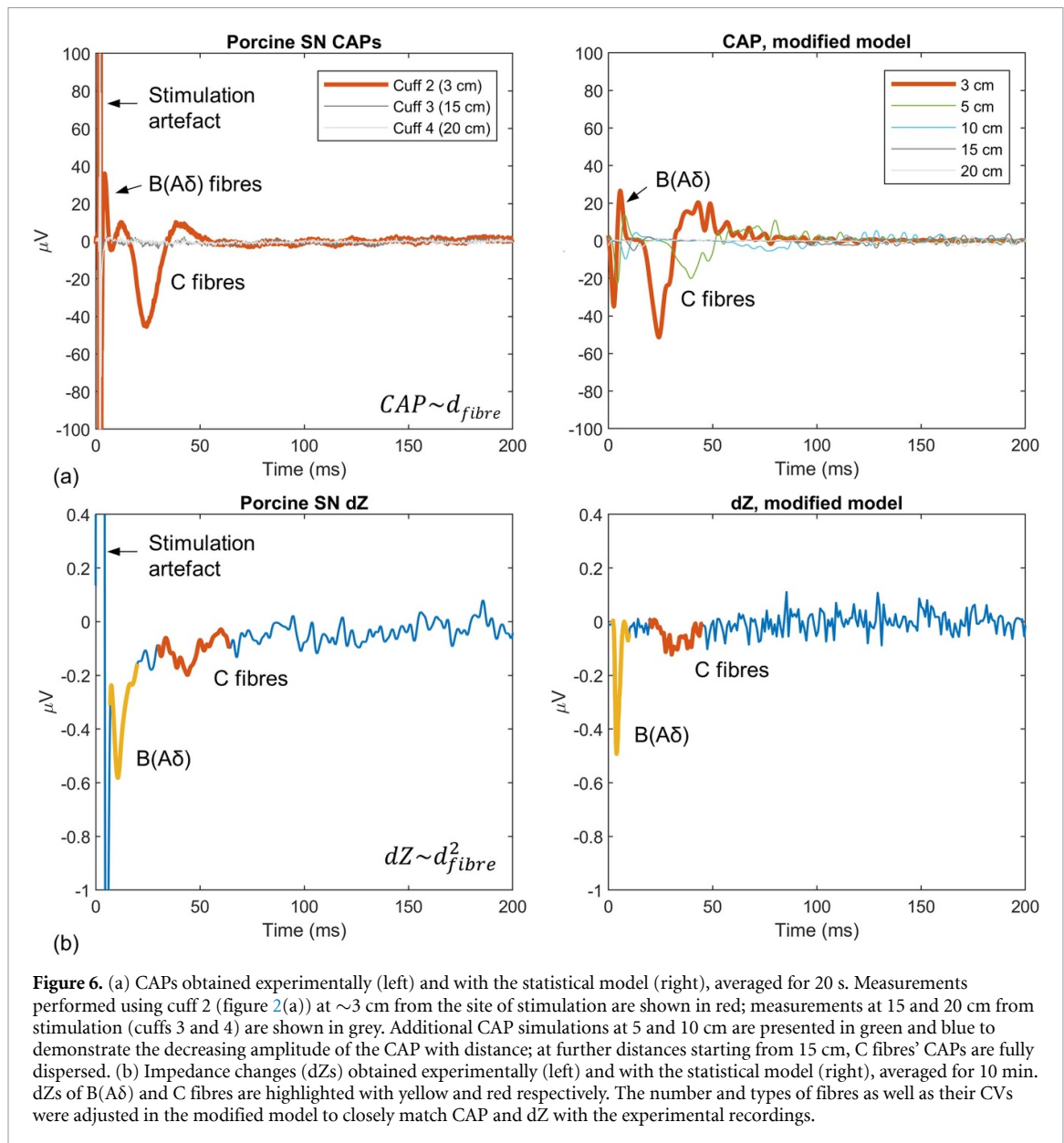
Figure 6. (a) CAPs obtained experimentally (left) and with the statistical model (right), averaged for 20 s. Measurements performed using cuff 2 (figure 2(a)) at ∼3 cm from the site of stimulation are shown in red; measurements at 15 and 20 cm from stimulation (cuffs 3 and 4) are shown in grey. Additional CAP simulations at 5 and 10 cm are presented in green and blue to demonstrate the decreasing amplitude of the CAP with distance; at further distances starting from 15 cm, C fibres' CAPs are fully dispersed. (b) Impedance changes (dZs) obtained experimentally (left) and with the statistical model (right), averaged for 10 min. dZs of B(Aδ) and C fibres are highlighted with yellow and red respectively. The number and types of fibres as well as their CVs were adjusted in the modified model to closely match CAP and dZ with the experimental recordings.

Table 3. Optimised stimulation and processing parameters used in the model.

Parameter	Value					
Stimulation (train) frequency	1 Hz	2 Hz	5 Hz	10 Hz	20 Hz	50 Hz
$N_{spikes/train}$	10	20	6	6	6	6
Duration of the train	10 s	10 s	1.2 s	0.6 s	0.3 s	0.15 s
Time between trains	0 s (continuous)			5 s		
Duration of the simulation			30 min			
$N_{trains/30\,min}$	180	180	163	327	480	553
Filtering bandwidth (single pulses)			200 Hz			
Corrected bandwidth (trains)			10 Hz			
Distances of measurement			3, 15, 20, 50 cm			

4. Discussion

4.1. Summary of results

(a) The statistical model of TD in porcine SN based on the FEM model of C nociceptor and morphometric data on this type of nerve was developed (figure 5, steps 1–3). The model was matched to the experimental recordings of CAPs and impedance changes measured in pig SNs at 3 cm from the stimulation *ex vivo*. The designed versatile model could accurately predict the shape and amplitude of the dispersed signals observed in porcine SN subjected to various stimulation paradigms.
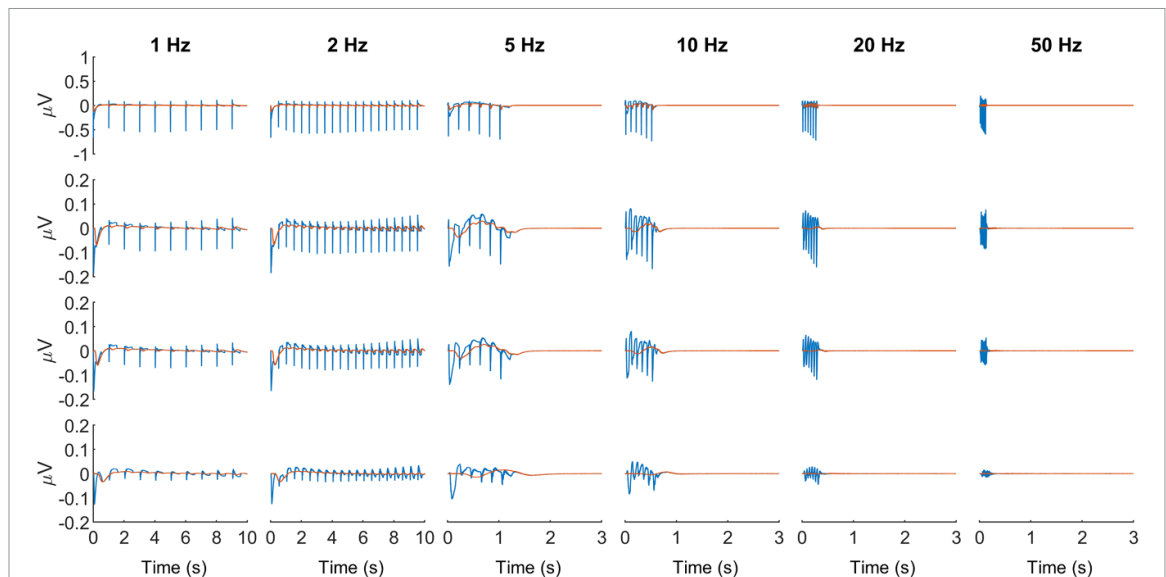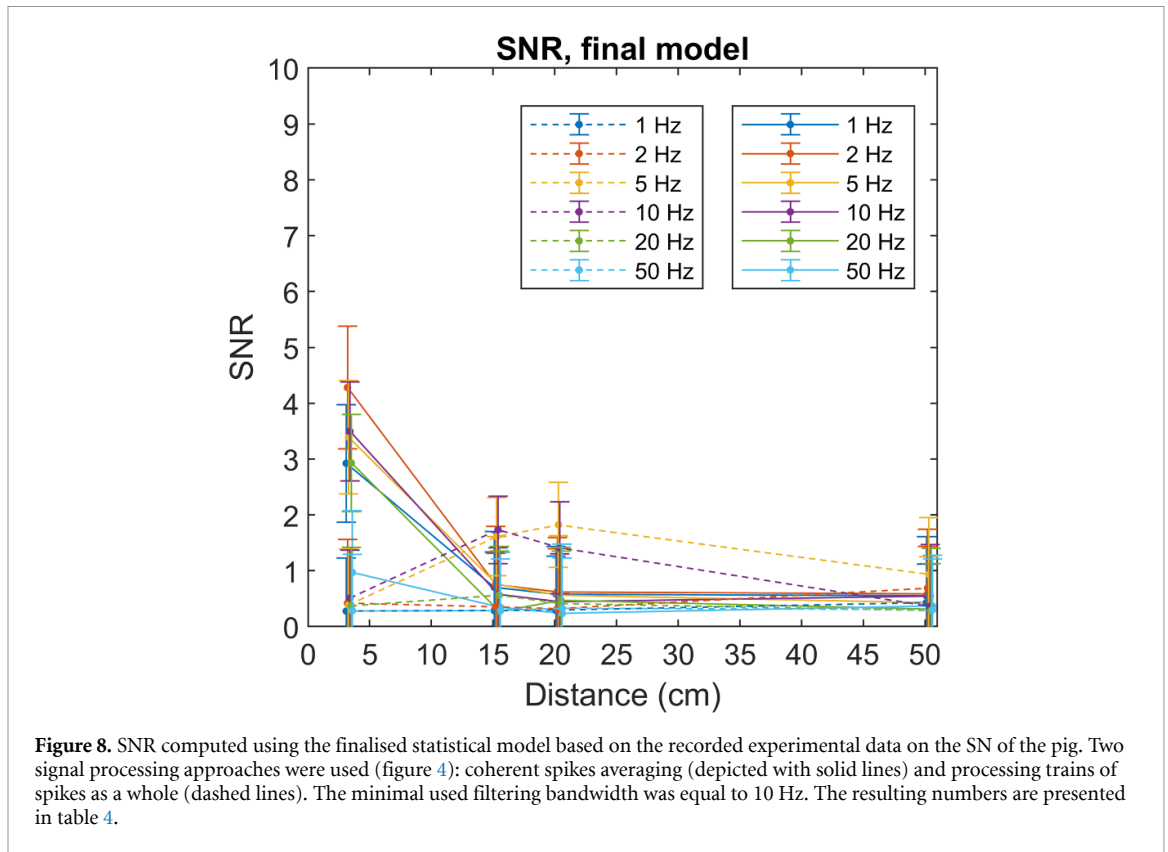
Figure 7. (Red lines) Dispersed dZs of an artificial unmyelinated nerve obtained with a statistical model containing 40 000 C-fibres, with EAP shape based on the cuff electrode design depicted on figure 1(b). The stimulation frequencies were 1, 2, 5, 10, 20 and 50 Hz (columns), and readings were made at 3, 15, 20 and 50 cm from the stimulus (rows). Resultant dZs were detrended after summation; noise was omitted for readability. (Blue lines) Dispersed dZs of a mixed nerve obtained with an experimentally adjusted statistical model containing 40 000 C-fibres and 4000 fast myelinated fibres.

Table 4. SNR simulated with the experimentally adjusted model after 30 min averaging.

Signal processing	Stimulation frequency	SNR (mean ± s.d.)[a]			
		3 cm	15 cm	20 cm	50 cm
Coherent spikes averaging	1 Hz	2.9 ± 1.1	0.7 ± 1.0	0.6 ± 0.9	0.6 ± 1.1
	2 Hz	4.3 ± 1.1	0.7 ± 1.0	0.6 ± 1.0	0.6 ± 0.8
	5 Hz	3.4 ± 1.0	0.8 ± 0.8	0.6 ± 1.1	0.4 ± 0.8
	10 Hz	3.5 ± 0.9	0.6 ± 0.8	0.4 ± 0.9	0.5 ± 0.9
	20 Hz	2.9 ± 0.9	0.3 ± 1.2	0.5 ± 0.9	0.3 ± 1.1
	50 Hz	1.0 ± 1.1	0.3 ± 1.0	0.2 ± 1.0	0.4 ± 0.9
Processing as trains	1 Hz	0.3 ± 1.0	0.3 ± 1.1	0.3 ± 1.0	0.4 ± 0.7
	2 Hz	0.4 ± 1.1	0.4 ± 1.0	0.3 ± 1.1	0.7 ± 1.1
	5 Hz	0.4 ± 1.0	1.6 ± 0.7	1.8 ± 0.8	0.9 ± 1.0
	10 Hz	0.5 ± 0.9	1.7 ± 0.6	1.4 ± 0.8	0.4 ± 0.8
	20 Hz	0.4 ± 1.1	0.6 ± 0.8	0.4 ± 1.0	0.3 ± 0.8
	50 Hz	0.3 ± 1.0	0.9 ± 0.3	0.3 ± 1.1	0.3 ± 0.9

[a] The stimulation frequencies where SNR ⩾ 1 and the optimal train frequencies are highlighted in blue

(b) The designed model was used for the development and optimisation of a novel stimulation and signal processing paradigm to record impedance changes in unmyelinated nerves at the distances from the stimulus where CAPs are dispersed (figure 5, step 4). This determined optimal paradigm was the following: 5 or 10 Hz trains with 6 pulses/train and 5 s interval between trains, and subsequent signal processing using 10 Hz band-pass filter to account for the presence of myelinated fibres, low-frequency noise and stimulation artefacts (table 1). The resulting SNR predicted with the model with stimulation by 10 Hz trains were 1.8 ± 0.8 and 1.4 ± 1.1 at 15 and 20 cm respectively (figure 8 and table 4). Thus, more than 30 min

of averaging would be required to record dZ further than 20 cm from the stimulus.

(c) The model's predictions were evaluated experimentally by stimulation of pig SNs by trains of stimuli *ex vivo* (figures 9, 5 and step 5). The predictions were in good agreement with the simulations: although the levels of noise were significantly reduced compared to the previous dZ measurement experiments [12], SNR obtained after 30 min of averaging (section 3) was at the edge of detectability at 15 and 20 cm from the onset of the stimulus. This was partly due to low-frequency noise and stimulation artefacts observed in the recordings that required increasing the bandwidth of filtering to a minimum of 10 Hz.

Figure 8. SNR computed using the finalised statistical model based on the recorded experimental data on the SN of the pig. Two signal processing approaches were used (figure 4): coherent spikes averaging (depicted with solid lines) and processing trains of spikes as a whole (dashed lines). The minimal used filtering bandwidth was equal to 10 Hz. The resulting numbers are presented in table 4.

4.2. Answers to the stated questions

(a) What are the optimal stimulation and signal processing strategies producing the largest impedance changes at different distances (15, 20 and 50 cm) from the onset?

The optimal stimulation strategies producing the largest impedance change signal are stimulation with 10 Hz trains, with 6 pulses per train and 5 s between trains, for the long-term survival of the nerve necessary for the desired chronic implantation. Other parameters were: AC current—200–300 μA amplitude, 1–1.5 kHz frequency, stimulation current—20–30 mA amplitude, 50 μs pulse width.
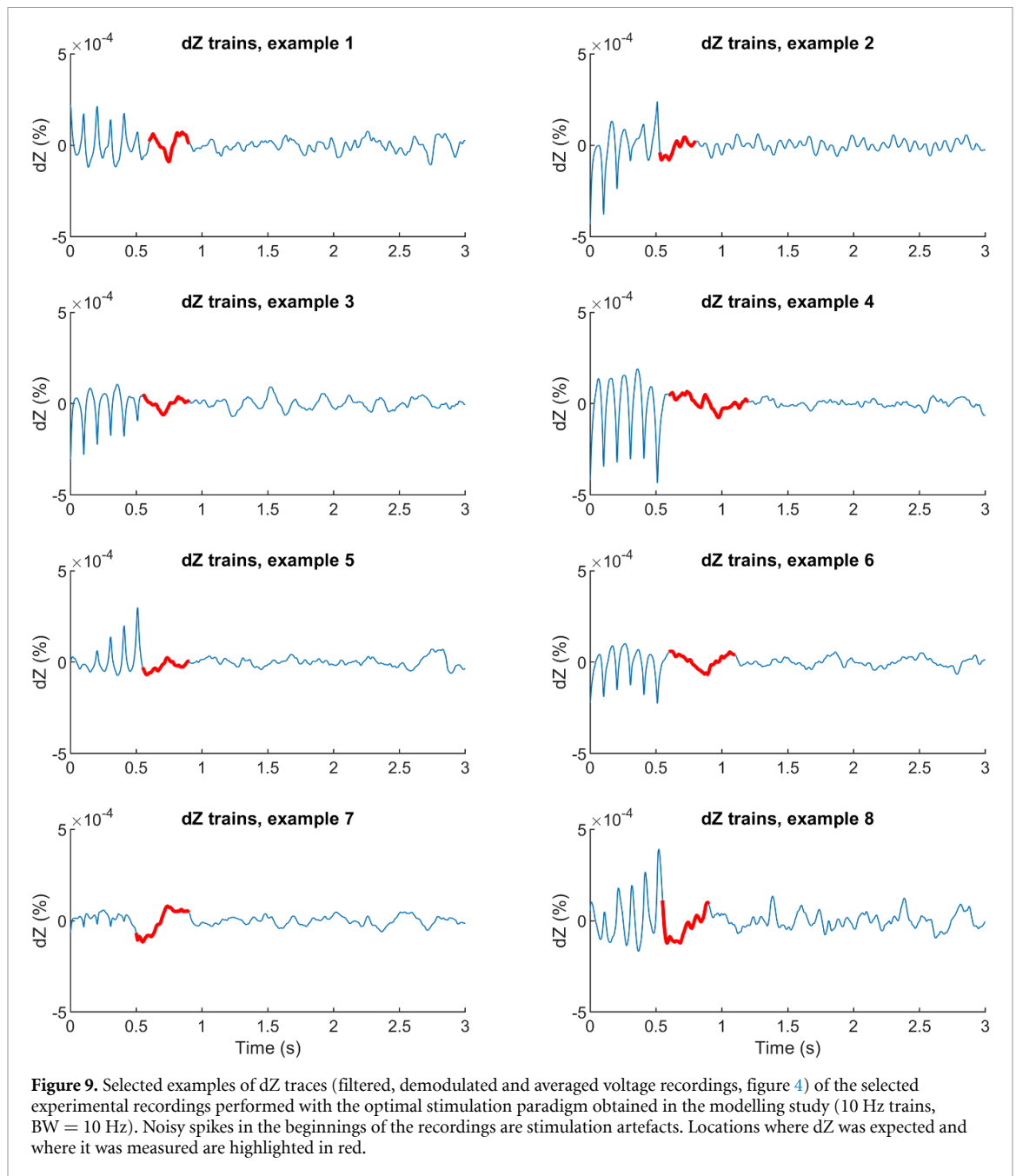
(b) How much averaging is required (1) to obtain a measurable signal (SNR > 1) and (2) to image neural activity with EIT (which requires SNR > 4 [18]) at 15, 20 and 50 cm from the site of stimulation?

Given the very low experimentally achieved noise of 3.5 μV RMS before averaging, the dZ in the porcine SN at 15–20 cm from the stimulus was at the edge of detectability (SNR < 2) if averaged for 30 min. To obtain larger SNR, longer averaging would be required. At 50 cm from the stimulus, to obtain SNR $\geqslant$ 2 one would need to average for approximately 1.5 h, given the noise decreases with the square root of the number of averages (table 4).

In order to image fast neural activity in fascicles of unmyelinated nerves in their cross-section, a minimal SNR of 4 obtained by sequential switching between 14 electrode pairs is required [18, 19]. Therefore, to achieve imaging with the obtained optimal paradigm, and considering that the noise decreases with the square root of the duration of averaging, the minimal averaging time would equal to 30 min $\cdot$ $(4/1.8)^2 \cdot$ 14 electrode pairs $\approx$ 34 h at 15 cm from the site of stimulation. This time would increase significantly for imaging at further distances in accordance with the table 4.

However, even such a long duration of averaging may be clinically feasible, for example, in implantable neuromodulation devices [2–4] that may run the specified stimulation paradigm for days or even weeks without any adverse effects to patients. In addition, if the internal organisation of the nerve being stimulated is known, for example, using the feedback system based on the physiological responses (such as respiratory breath rate or heart rate) following stimulation with multi-electrode cuff arrays [51], there is no need in the execution of a full imaging paradigm with 14 electrode pairs. Instead, one could concentrate on specific electrode pairs corresponding to the required fascicles that may help to decrease the duration of averaging by two- or three-fold.

In addition, future plans include transitioning to an *in vivo* experimental paradigm which has several potential advantages over the *ex vivo* one used in the

Figure 9. Selected examples of dZ traces (filtered, demodulated and averaged voltage recordings, figure 4) of the selected experimental recordings performed with the optimal stimulation paradigm obtained in the modelling study (10 Hz trains, BW = 10 Hz). Noisy spikes in the beginnings of the recordings are stimulation artefacts. Locations where dZ was expected and where it was measured are highlighted in red.

current study. Although the level of noise is expected to increase *in vivo* (to 8–10 μV before averaging [12, 19]), the SNR may be improved (given enough averaging) for the following reasons:

- The contact between the cuff and the nerve should improve due to the absence of saline solution in and around the cuffs, and this will lead to stronger signals.
- The whole length of the VNS can be utilised *in vivo* that will significantly reduce stimulation artefacts strongly affecting the recorded dZ signals.

In the anaesthetized animal, stimulation can be done in the cervical part of the nerve while the recording cuff can be placed in the subdiaphragmatic

part. This was not possible to perform *ex vivo* due to the limited size of the nerve bath and complex surgical procedures required to remove longer parts of the nerve from the body. Removal of stimulation artefacts will enable measurement of the whole duration of the compound dZ signals, and not just the ending parts which follow stimulation artefacts (figure 9), and this is expected to strongly improve the SNR.

Even with such a long averaging expected to be required for EIT imaging, the new experimental paradigm developed in the study demonstrates the feasibility of recording impedance changes far from the site of stimulation, which cannot be currently achieved using other existing methods.

(c) Are simulated results confirmed with experimental data?

The SNR measured in the performed *ex-vivo* experiments were in agreement with the values obtained with the developed model of dispersion (figures 8, 9 and section 3)). With the average level of noise achieved in the developed experimental setup (3.5 μV RMS), the maximal distance from the onset where significant reproducible dZ could be measured in 30 min was 15 cm.

4.3. Limitations
The current study had several limitations. First, it was the statistical model and not the FEM model which was used for simulation of dispersion in unmyelinated nerves and for obtaining the optimal parameters for dZ measurement. Since computational time and the amount of required resources rise exponentially with the number of fibres in the FEM model, FEM simulation of 40 thousand-fibre nerve would be very computationally intensive and will demand unrealistic time and resources. For instance, it takes about an hour for a 40 ms simulation of the single C fibre FEM model described by a system of 20 differential equations, while a model with 50 fibres of the same type required a whole week on a double-CPU machine with 128 Gb RAM [22]. However, the statistical model was based on the signals simulated with the realistic mammalian C fibre FEM model that brought them into accordance with real experimental data.

Second, the FEM model was not solved for each fibre location in the cross-section of the cylindrical external space, so that the simulations were performed only for the fibre placed in the centre. This was done for two main reasons. First, the system was symmetric (1 μm fibre in the centre of 10 μm external space), so that placement of the fibre in other positions inside the cylinder could be assumed to not significantly alter the shape of the measured signal but to mainly affect its amplitude. Also, during the transition to the multi-fibre statistical model, the diameter of the cuff was re-adjusted so that the uniformly distributed fibres were on average equidistant from the electrodes (supplementary material, equation (3A)), and the error brought by small variations in the shapes of single APs is not expected to significantly contribute into the error of the resultant CAP. In addition, this simplification allowed to significantly reduce computational time: in the current study, the fibre was stimulated with trains of pulses lasting up to 10 s (table 1) that took up to 40 h per single simulation.

Third, the porcine SNs used in the *ex-vivo* experimental study were short, of up to 20 cm long, that led to large stimulation artefacts overlapping with the dZ measured at these distances. In addition, since around 10% of the porcine SN consists of fast and large myelinated fibres producing larger dZ, they produce the artefactual signal of the same kind as stimulation appearing during the initial phase of the dispersed signal (figure 7). Therefore, only the ending part of the dispersed dZ not covered under these artefacts had to be studied (figure 9), and the SNR may have thus been reduced. One way to significantly reduce these artefacts is to use longer nerves, and this can be achieved in the *in vivo* experiments which are planned as the next step of the presented study.

4.4. Future work
In order to remove or significantly reduce the stimulation artefacts and the artefacts caused by the presence of the myelinated fibres, the future work will be to perform an experimental study in paralysed pigs *in vivo* with stimulation on the cervical part of the VNS and recording on the subdiaphragmatic part which is around one metre apart. This will allow measurement of the pure dZ signal not contaminated by this type of artefact. In addition, *in vivo* setup may provide better contact between the cuff electrodes and the nerve due to the absence of a highly conductive saline interface present in the *ex vivo* bath; this will potentially lead to larger signals and the SNR.

5. Conclusion

It is challenging to measure CAPs and impedance changes in unmyelinated nerves starting from a few centimetres from the site of stimulation. The developed experimentally adjusted computational model of TD in nerve allowed simulation of compound APs and dZs at various distances from the variable stimulus. With the model, optimal stimulation and signal processing parameters for dZ measurement were determined. It was shown that stimulation of the nerve by trains of stimuli allows recording impedance changes further from the onset than it is possible with a traditional continuous stimulation and averaging of consecutive spikes. The findings were evaluated experimentally using the porcine SN *ex vivo*. This work enables a new way for measurement of impedance changes accompanying excitation at distances from the stimulation where standard approaches are not feasible.

The models of dispersion in complex-fibre nerves designed for optimisation of the experimental parameters in the current study can be used by research community for studying the dispersion-related properties in any types of nerves and the development of novel techniques for sensing neural activity in unmyelinated nerves. The latter can be particularly useful for facilitation of the novel field of bioelectronic medicines aimed at neuromodulation of internal organs via stimulation of the VNS: development of novel closed-loop solutions involving stimulation of the nerve in response to the recorded physiological signals will enhance the treatment outcomes for a variate of drug-resistant disorders including, among

others, epilepsy, depression, and cardiovascular diseases.

Data availability statement

The data that support the findings of this study are available upon reasonable request from the authors.

The COMSOL and MATLAB model files used for FEM and statistical modelling, as well as the MATLAB code written for data processing are provided online in the EIT-lab GitHub repository [43]. All the recorded unprocessed data will be available online in the SPARC portal (https://sparc.science/) after approval.

Acknowledgments

ORCID iDs

Ilya Tarotin ⬤ https://orcid.org/0000-0001-7928-6053
Svetlana Mastitskaya ⬤ https://orcid.org/0000-0002-4819-2908
Enrico Ravagli ⬤ https://orcid.org/0000-0002-4874-9366
David Holder ⬤ https://orcid.org/0000-0003-2755-6124
Kirill Aristovich ⬤ https://orcid.org/0000-0002-2924-5680

References

[1] Waltz E 2016 A spark at the periphery *Nat. Biotechnol.* **34** 904–8

[2] González H F J, Yengo-Kahn A and Englot D J 2019 Vagus nerve stimulation for the treatment of epilepsy *Neurosurg. Clin. N. Am.* **30** 219–30

[3] Mulders D M, de Vos C C, Vosman I and van Putten M J A M 2015 The effect of vagus nerve stimulation on cardiorespiratory parameters during rest and exercise *Seizure* **33** 24–28

[4] Conway C R, Kumar A, Xiong W, Bunker M, Aaronson S T and Rush A J 2018 Chronic vagus nerve stimulation significantly improves quality of life in treatment-resistant major depression *J. Clin. Psychiatry* **79** 22269

[5] Sabbah H N, Ilsar I, Zaretsky A, Rastogi S, Wang M and Gupta R C 2011 Vagus nerve stimulation in experimental heart failure *Heart Fail. Rev.* **16** 171–8

[6] Koopman F A *et al* 2016 Vagus nerve stimulation inhibits cytokine production and attenuates disease severity in rheumatoid arthritis *Proc. Natl Acad. Sci.* **113** 8284–9

[7] Bonaz B, Sinniger V and Pellissier S 2016 Anti-inflammatory properties of the vagus nerve: potential therapeutic implications of vagus nerve stimulation *J. Physiol.* **594** 5781–90

[8] Rosas-Ballina M, Ochani M, Parrish W R, Ochani K, Harris Y T, Huston J M, Chavan S and Tracey K J 2008 Splenic nerve is required for cholinergic antiinflammatory pathway control of TNF in endotoxemia *Proc. Natl Acad. Sci. USA* **105** 11008–13

[9] Borovikova L V, Ivanova S, Zhang M, Yang H, Botchkina G I, Watkins L R, Wang H, Abumrad N, Eaton J W and Tracey K J

2000 Vagus nerve stimulation attenuates the systemic inflammatory response to endotoxin *Nature* **405** 458–62

[10] Ben-Menachem E 2002 Vagus-nerve stimulation for the treatment of epilepsy *Lancet Neurol.* **1** 477–82

[11] Klinkenberg S, Aalbers M W, Vles J O H A N S H, Cornips E R W I N M J, Rijkers K, Leenen L, Kessels F O N S G H, Aldenkamp A P and Majoie M 2012 Vagus nerve stimulation in children with intractable epilepsy: a randomized controlled trial *Dev. Med. Child Neurol.* **54** 855–61

[12] Aristovich K, Donegá M, Blochet C, Avery J, Hannan S, Chew D J and Holder D 2018 Imaging fast neural traffic at fascicular level with electrical impedance tomography: proof of principle in rat sciatic nerve *J. Neural Eng.* **15** 056025

[13] Aristovich K Y, Packham B C, Koo H, Dos Santos G S, McEvoy A and Holder D S 2016 Imaging fast electrical activity in the brain with electrical impedance tomography *NeuroImage* **124** 204–13

[14] Hannan S, Faulkner M, Aristovich K, Avery J, Walker M C and Holder D S 2020 *In vivo* imaging of deep neural activity from the cortical surface during hippocampal epileptiform events in the rat brain using electrical impedance tomography *NeuroImage* **209** 116525

[15] Ravagli E, Mastitskaya S, Thompson N, Aristovich K and Holder D 2019 Optimization of the electrode drive pattern for imaging fascicular compound action potentials in peripheral nerve with fast neural electrical impedance tomography *Physiol. Meas.* **40** 115007

[16] Avery J, Dowrick T, Faulkner M, Goren N and Holder D 2017 A versatile and reproducible multi-frequency electrical impedance tomography system *Sensors* **17** 280

[17] Fabrizi L, McEwan A, Woo E and Holder D S 2007 Analysis of resting noise characteristics of three EIT systems in order to compare suitability for time difference imaging with scalp electrodes during epileptic seizures *Physiol. Meas.* **28** S217–36

[18] Gilad O and Holder D S 2009 Impedance changes recorded with scalp electrodes during visual evoked responses: implications for electrical impedance tomography of fast neural activity *NeuroImage* **47** 514–22

[19] Ravagli E, Mastitskaya S, Thompson N, Iacoviello F, Shearing P R, Perkins J, Gourine A V, Aristovich K and Holder D 2020 Imaging fascicular organization of rat sciatic nerves with fast neural electrical impedance tomography *Nat. Commun.* **11** 1–10

[20] Faulkner M, Hannan S, Aristovich K, Avery J and Holder D 2018 Feasibility of imaging evoked activity throughout the rat brain using electrical impedance tomography *NeuroImage* **178** 1–10

[21] Hope J, Aqrawe Z, Lim M, Vanholsbeeck F and McDaid A 2019 Increasing signal amplitude in electrical impedance tomography of neural activity using a parallel resistor inductor capacitor (RLC) circuit *J. Neural Eng.* **16** 066041

[22] Tarotin I, Aristovich K and Holder D 2019 Effect of dispersion in nerve on compound action potential and impedance change: a modelling study *Physiol. Meas.* **40** 034001

[23] Shimizu T, Hayashi M, Kawata A, Mizutani T, Watabe K and Matsubara S 2011 A morphometric study of the vagus nerve in amyotropic lateral sclerosis with circulatory collapse *Amyotroph. Lateral Scler.* **12** 356–62

[24] Prechtl J C and Powley T L 1987 A light and electron microscopic examination of the vagal hepatic branch of the rat *Anat. Embryol.* **176** 115–26

[25] Coleridge J C G and Coleridge H M 1984 Afferent vagal C fibre innervation of the lungs and airways and its functional significance *Rev. Physiol. Biochem. Pharmacol.* **99** 1–110

[26] Freeman W J J 1972 Spatial divergence and temporal dispersion in primary olfactory nerve of cat *J. Neurophysiol.* **35** 733–44

[27] Olney R K, Budingen H J and Miller R G 1987 The effect of temporal dispersion on compound action potential area in human peripheral nerve *Muscle Nerve* **10** 728–33

[28] Dorfman L J 1984 The distribution of conduction velocities (DCV) in peripheral nerves: a review *Muscle Nerve* **7** 2–11

[29] Schulte-Mattler W J, Müller T, Georgiadis D, Kornhuber M E and Zierz S 2001 Length dependence of variables associated with temporal dispersion in human motor nerves *Muscle Nerve* **24** 527–33

[30] Chang R B, Strochlic D E, Williams E K, Umans B D and Liberles S D 2015 Vagal sensory neuron subtypes that differentially control breathing *Cell* **161** 622–33

[31] Settell M L *et al* 2020 Functional vagotopy in the cervical vagus nerve of the domestic pig: implications for the study of vagus nerve stimulation *J. Neural Eng.* **17** 026022

[32] Thompson N, Mastitskaya S and Holder D 2019 Avoiding off-target effects in electrical stimulation of the cervical vagus nerve: neuroanatomical tracing techniques to study fascicular anatomy of the vagus nerve *J. Neurosci. Methods* **325** 108325

[33] Chapman C A R *et al* 2019 Optimisation of bioimpedance measurements of neuronal activity with an ex vivo preparation of Cancer pagurus peripheral nerves *J. Neurosci. Methods* **327** 108322

[34] Chapman C A R, Aristovich K, Donega M, Fjordbakk C T, Stathopoulou T-R, Viscasillas J, Avery J, Perkins J D and Holder D 2019 Electrode fabrication and interface optimization for imaging of evoked peripheral nervous system activity with electrical impedance tomography (EIT) *J. Neural Eng.* **16** 016001

[35] Tarotin I, Mastitskaya S, Hannan S, Ravagli E, Aristovich K and Holder D 2020 SPARC: method for overcoming temporal dispersion in unmyelinated nerves for imaging C fibres with electrical impedance tomography (EIT) *FASEB J.* **34** 1

[36] Tarotin I, Aristovich K and Holder D 2019 Model of impedance changes in unmyelinated nerve fibers *IEEE Trans. Biomed. Eng.* **66** 471–84

[37] Stakenborg N, Gomez-Pinilla P J, Verlinden T J M, Wolthuis A M, D'Hoore A, Farré R, Herijgers P, Matteoli G and Boeckxstaens G E 2020 Comparison between the cervical and abdominal vagus nerves in mice, pigs, and humans *Neurogastroenterol. Motil.* **32** 1–8

[38] Tigerholm J, Petersson M E, Obreja O, Lampert A, Carr R, Schmelz M and Fransén E 2014 Modeling activity-dependent changes of axonal spike conduction in primary afferent C-nociceptors. *J. Neurophysiol.* **111** 1721–35

[39] Cole K S and Curtis H J 1939 Electric impedance of the squid giant axon during activity. *J. Gen. Physiol.* **22** 649–70

[40] Tarotin I, Aristovich K and Holder D 2019 Simulation of impedance changes with a FEM model of a myelinated nerve fibre *J. Neural Eng.* **16** 056026

[41] Boyd I A and Kalu K U 1979 Scaling factor relating conduction velocity and diameter for myelinated afferent nerve fibres in the cat hind limb. *J. Physiol.* **289** 277–97

[42] Soltanpour N and Santer R M 1996 Preservation of the cervical vagus nerve in aged rats: morphometric and enzyme histochemical evidence *J. Auton. Nervous Syst.* **60** 93–101

[43] Tarotin Ilya 2021 *GitHub* (available at: https://github.com/EIT-team/Overcoming-dispersion-trains)

[44] Scriven D R 1981 Modeling repetitive firing and bursting in a small unmyelinated nerve fiber *Biophys. J.* **35** 715–30

[45] Zhong Y, Wang J, Beckel J, De Groat W and Tai C 2021 Model analysis of post-stimulation effect on axonal conduction and block *IEEE Trans. Biomed. Eng.* **9294** 1

[46] Brown E A, Ross J D, Blum R A, Nam Y, Wheeler B C and DeWeerth S P 2008 Stimulus-artifact elimination in a multi-electrode system *IEEE Trans. Biomed. Circuits Syst.* **2** 10–21

[47] Shadmani A, Viswam V, Chen Y, Bounik R, Dragas J, Radivojevic M, Geissler S, Sitnikov S, Muller J and Hierlemann A 2019 Stimulation and artifact-suppression techniques for *in vitro* high-density microelectrode array systems *IEEE Trans. Biomed. Eng.* **66** 2481–90

[48] Kagiava A and Theophilidis G 2011 High concentrations of dichloroacetate have minor effects on the vitality of the mammalian nerve fibers *Anti-Cancer Drugs* **22** 273–6

[49] Bastian C, Brunet S and Baltan S 2020 Ex vivo studies of optic nerve axon electrophysiology *Methods Mol. Biol.* **2143** 169–77

[50] Aristovich K Y, Dos Santos G S and Holder D S 2015 Investigation of potential artefactual changes in measurements of impedance changes during evoked activity: implications to electrical impedance tomography of brain function *Physiol. Meas.* **36** 1245–59

[51] Aristovich K *et al* 2021 Model-based geometrical optimisation and *in vivo* validation of a spatially selective multielectrode cuff array for vagus nerve neuromodulation *J. Neurosci. Methods* **352** 109079